PROTEINS
STRUCTURE ■ FUNCTION ■ BIOINFORMATICS

Novel high-affinity binders of human interferon gamma derived from albumin-binding domain of protein G

Jawid N. Ahmad,[1†] Jingjing Li,[2†] Lada Biedermannová,[2] Milan Kuchař,[2] Hana Šípová,[3] Alena Semerádtová,[4] Jiří Černý,[2] Hana Petroková,[2] Pavel Mikulecký,[2] Jiří Polínek,[2] Ondřej Staněk,[1] Jiří Vondrášek,[2] Jiří Homola,[3] Jan Malý,[4] Radim Osička,[1] Peter Šebo,[1,2] and Petr Malý[2*]

[1] Institute of Microbiology of the ASCR, v. v. i., Vídeňská 1083, 142 20 Prague, Czech Republic
[2] Institute of Biotechnology of the ASCR, v. v. i., Vídeňská 1083, 142 20 Prague, Czech Republic
[3] Institute of Photonics and Electronics of the ASCR, v. v. i., Chaberská 57, 182 51 Prague, Czech Republic
[4] Faculty of Science, Jan Evangelista Purkyně University, České Mládeže 8, 400 96 Ústí nad Labem, Czech Republic

ABSTRACT

Recombinant ligands derived from small protein scaffolds show promise as robust research and diagnostic reagents and next generation protein therapeutics. Here, we derived high-affinity binders of human interferon gamma (hIFNγ) from the three helix bundle scaffold of the albumin-binding domain (ABD) of protein G from *Streptococcus* G148. Computational interaction energy mapping, solvent accessibility assessment, and *in silico* alanine scanning identified 11 residues from the albumin-binding surface of ABD as suitable for randomization. A corresponding combinatorial ABD scaffold library was synthesized and screened for hIFNγ binders using *in vitro* ribosome display selection, to yield recombinant ligands that exhibited K_d values for hIFNγ from 0.2 to 10 n*M*. Molecular modeling, computational docking onto hIFNγ, and *in vitro* competition for hIFNγ binding revealed that four of the best ABD-derived ligands shared a common binding surface on hIFNγ, which differed from the site of human IFNγ receptor 1 binding. Thus, these hIFNγ ligands provide a proof of concept for design of novel recombinant binding proteins derived from the ABD scaffold.

Proteins 2012; 80:774–789.

Key words: recombinant ligand; protein scaffold; computational design; combinatorial library; ribosome display.

INTRODUCTION

Interferon gamma is a pro-inflammatory cytokine that plays a key role in innate immune response.[1–3] It consists of a 143 residue-long all-alpha glycoprotein forming a head-to-tail dimer[4,5] in which four of the six helices of one subunit are interlocked with two of the helices of the other subunit. This yields a globular homodimer structure with a noncrystallographic twofold axis.[6]

Currently, specific antibodies are used for determination of levels of human interferon gamma (hIFNγ) released by activated antigen-specific memory T cells, such as in the commercial enzyme-linked immunosorbent assay (ELISA) or ELISPOT assays for detection of latent tuberculosis infection. In turn, development of microfluidic biosensors for hIFNγ, or other bioanalytes, often requires the use of alternative and more robust reagents that can resist reducing conditions, hydrodynamic shearing forces and/or refold quantitatively upon denaturation. These are typically small engineered binding proteins (recombinant ligands), which are nowadays intensely explored as an alternative to antibodies for many applications.[7–9]

Because of the complexity of the folding problem, however, de novo design of proteins with desirable properties remains difficult. Therefore, engineering of protein scaffolds with robustly organized structure has been used to generate recombinant ligands.[8,10–13] Protein domains that are stable enough to tolerate amino acid substitutions without losing the original fold have, indeed, successfully been used for generation of highly complex libraries of randomized scaffold variants.[7,12,14,15] These were subsequently screened for binders of numerous targets, using high-

[†]Jawid N. Ahmad and Jingjing Li contributed equally to this work.

Grant sponsor: Grant Agency of The Academy of Sciences of the Czech Republic; Grant number: KAN200520702; Grant sponsor: Grant Agency of the Czech Republic; Grant number: P305/10/2184; Grant sponsor: Academy of Sciences of the Czech Republic, Institutional Research Concept; Grant numbers: AV0Z50200510 and AV0Z50520701.
*Correspondence to: Petr Malý, Institute of Biotechnology of the ASCR, v. v. i., Vídeňská 1083, 142 20 Praha 4, Czech Republic. E-mail: petr.maly@img.cas.cz.
Received 16 August 2011; Revised 5 October 2011; Accepted 17 October 2011
Published online 29 October 2011 in Wiley Online Library (wileyonlinelibrary.com).
DOI: 10.1002/prot.23234

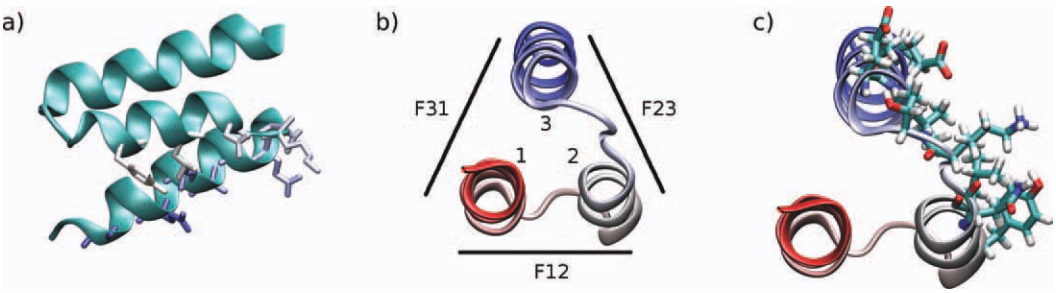

Figure 1

The ABD scaffold. (**a**) ABD protein structure in ribbon representation, with the 11 residues selected for randomization shown as sticks. (**b**) Definition of the three faces of the ABD molecule. (**c**) ABD protein structure with indicated randomized residues in the same orientation as in (b).

throughput selection technologies, such as phage or cell surface display *in vivo*,[16] or display of nascent proteins on ribosomes *in vitro*.[17] Typically, the diversification of a scaffold sequence involves combinatorial randomization at certain positions[8] and affinity maturation of selected binders by a combination of semirational and random mutagenesis procedures.[18] The bottleneck of these approaches, however, is the choice of residues for randomization, so as to preserve the stability and folding of the scaffold.[15] Toward this aim, empirical,[7] structure-instructed,[8] and "consensus design" approaches have been used,[19] with the latter allowing successful construction of combinatorial DARPin libraries.[20,21] In these approaches, however, some of the positions suitable for randomization may be missed, as conservation of function and structure are particularly hard to distinguish in globular proteins and mutations of surface residues can affect protein stability. On the other hand, the surface of most protein scaffolds appears to contain residue patches where extensive sequence variation does not affect the overall structure.[22]

In this study, we analyzed the potential to serve as a binder scaffold for a 46 residue-long segment from the third albumin-binding domain (ABD) of protein G from *Streptococcus* G148 (SpG), also called the GA module (PDB ID: 1GJT, residues 20–65). This left-handed three-helix bundle domain binds human serum albumin (HSA) with nanomolar affinity[23–25] and exhibits a 3D structure that resembles a trigonal prism, with edges formed by the three helices [Fig. 1(a–c)]. Previous alanine scanning experiments revealed that residues contributing the affinity for HSA were located on the face F23.[26] Indeed, structural analysis of the HSA complex with the ALB8_GA protein of *Finegoldia magna* (PDB ID: 1TF0) confirmed that residues from the second ABD helix and the loops surrounding it are involved in HSA binding together with residues from helix 3.[27]

In a recent study, ABD library was constructed by randomization of 15 surface residues, based on structural and sequence conservation analysis, resulting in HSA-binders with 50–500 femtomolar affinities.[28] Moreover, a high thermal ($T_m \approx 70^\circ C$) and chemical stability was reported for ABD, which further qualified it as a candidate for construction of scaffold libraries. Recently, a dual affinity binder was constructed using randomization of ABD scaffold and phage display selection.[29]

In this work, we explored the potential of the ABD scaffold to yield binders of other targets than HSA. Toward this aim, rational selection of ABD residues amenable for randomization was complemented by computational analysis of structural stability of ABD upon *in silico* mutagenesis, so as to instruct the construction of a combinatorial library of ABD scaffolds. A highly mutable contiguous residue patch on the ABD surface was identified, which upon randomization and ribosome display selection yielded ligands that bind hIFNγ with nanomolar affinities.

MATERIALS AND METHODS

Interaction energy map

The structure of the third ABD of protein G from *Streptococcus* strain G148 was obtained from Protein Data Bank under accession code 1GJT. Its residues 20–65, marked here as ABD sequence, were used for structure modeling, with the numbering of residues 1–46 corresponding to the truncated sequence throughout this article.

For identification of the key stabilizing residues in the ABD structure, we used the interaction energy map (IEM) method, which evaluates the importance of each residue in protein structure based on the amount of stabilization energy the residue brings to the stability of the fold.[30] Standard parm94 force field[31] was applied as implemented in Amber 8 package,[32] together with the generalized Born solvent model,[33] using the standard value of dielectric constant of $\varepsilon_r = 78.5$ for water.

To calculate the individual residue–residue interactions in Amber, the polypeptide chain was split into fragments, cutting the peptide bond, and capping the fragments

with acetyl group ($H_3C—C=O—$) at the N terminus and with N-methyl group ($—NH—CH_3$) at the C terminus. The stabilization energy of *n*th residue was then calculated as the sum of all its pair-wise interaction energies in pairs of *n*th and *m*th residue, such as $|n - m| > 2$ (i.e., non-neighboring residues). Amber 8 package[32] and our own script were used for the calculations.

Calculation of solvent accessibility

The solvent-accessible surface area (SASA) of each residue in the ABD structure was calculated using the Parameter OPtimized Surfaces (POPS) web server[34,35] with atomic-level resolution algorithm and parameters.

In silico alanine scanning using Eris

The Eris protein stability estimator was used to predict the thermodynamic stability of the ABD fold following *in silico* mutation at certain positions.[36] This enables to accurately compute stability changes of proteins upon mutations using the protein-modeling force field Medusa, based on physical descriptions of atomic interactions and not relying on parameter training with available experimental protein stability data. The freely available Eris web server was used for calculations[37] with backbone prerelaxation option and backbone flexibility allowed.

Generation of DNA library

HPLC-purified synthetic oligonucleotides were used. The forward primer ABDLIB-setB1c (5′-TTAGC TGAAG CTAAA GTCTT AGCTA ACAGA GAACT TGACA AATAT GGAGT AAGTG AC-3′) and the reverse primer setB-rev (5′-ACCGCGGATC CAGGTAA-3′) were used for PCR in 10 times higher molar concentration than the connecting ABDLIB-setB2c template oligonucleotide. The latter had distinct codons randomized at defined positions (5′-ACCGCGGATCCAGGTAAMNNAGCTAAAATM NNATCTATMNNMNNTTTTACMNNMNNAACMNNM NNGGCMNNGTTGATMNNGTTCTTGTAMNNGTCAC TTACTCCATATTTGTC-3′), in which M represents C/A, N any nucleotides out of A, G, C or T. In order to prepare the DNA template for ribosome display, a published protocol[38] was used with slight modifications. To serve as a protein spacer for ribosome display, the *tolA* gene (GENE ID: 946625 tolA) coding for a membrane anchored protein from the TolA-TolQ-TolR complex was amplified from *Escherichia coli* K12 strain genomic DNA, using the primer pairs ABDLIB-tolA-link (5′-TTACCTGGATCCGCGGTCGGTTCGAGCTC-CAAGCTTGGATCTGGT GGCCAGAAGCAA-3′) and tolArev (5′-TTTCCGCTCGAGCTACGGTTT GAAGTC-CAATGGCGC-3′). The obtained products were linked to the randomized ABD sequences using amplification with primer pairs EWT5-ABDfor1 (5′-TTCCTCCATGG GTATGAGAGGATCGCATCACCATCACCATCACTTAGC TGAAGCTAAAGTCTTA-3′) and tolArev. The primer EWT5-ABDfor1 contains a sequence encoding a tetrapeptide MetArgGlySer and a six histidine tag fused to the N-terminus of the ABD. To add the T7 promoter and ribosome binding site sequences, the obtained DNA fragment was subjected to further consecutive PCR amplifications with the set of primers T7B (5′-ATACGAAATTAATACGACTCACTATAGGGAGACCACA ACGG-3′), SD-EW (5′-GGGAG ACCACAACGGTTTCC CTCTAGAAAT AATTTTGTTTAACTTTAAGAAGGAG A TATACCATGGGTATGAGAGGATCG-3′) and *tolA*k (5′-CCGCACACCAGTAAGGTGTG CGGTTTCAGTTGCCG CTTTCTTTCT-3′), generating a DNA library of ABD variants lacking the downstream stop codon.

Ribosome display selection

An aliquot of the generated DNA library with an estimated complexity of 10^{13} ABD allele variants was used for *in vitro* transcription reaction and the resulting mRNA was translated using *E. coli* S30 extract as described.[38] The translated products were loaded into microtiter plate wells precoated with 3% bovine serum albumin (BSA) for a preselecting subtraction of BSA-binding ligands at 4°C for 1 h, before transfer into Maxisorp (NUNC, Denmark) microtiter plate wells coated with recombinant hIFNγ and blocked with BSA. After incubation at 4°C for 1 h, the plate wells were washed three times with TBS (50 m*M* Tris-HCl pH 7.4, 150 m*M* NaCl), followed by washing with ice-cold WBT (50 m*M* Tris-acetate, pH 7.0, 150 m*M* NaCl, 50 m*M* MgAc) with increasing concentrations of Tween-20. To release mRNA from the bound ribosome complex, elution with elution buffer (50 m*M* Tris-acetate, pH 7.5, 150 m*M* NaCl, 50 m*M* ethylenediaminetetraacetic acid (EDTA)) containing 50 μg/mL of *Saccharomyces cerevisiae* RNA as carrier was performed. Purified RNA was transcribed into cDNA using a specific reverse transcription with setB-rev reverse primer, annealing to the 3′ end of the ABD cDNA. Double-strand DNA was next obtained by PCR using EWT5-ABDfor1 and setB-rev primers. The final amplified DNA encoding selected ABD variants contained T7 promoter and RBS sequences and a truncated *tolA* fragment. To isolate high affinity binders, the stringency of binding and washing conditions was increased after each round of selection (Table I).

ELISA screening for hIFNγ binders

DNA encoding ABD variants isolated after the final round of selection was fused with full-length *tolA* sequence using PCR amplification with the EWT5-ABD-for1 and tolArev primer pair. The resulting DNA product was digested with *Nco*I and *Xho*I enzymes, ligated into the pET28b plasmid, and transformed into *E. coli* DH5α. For production of the 6×His-ABD-tolA fusion products,

Table I
Stringency of Washing Conditions Used in Each Cycle of Ribosome Display

Cycle number	1	2	3	4	5[a]	6	7[b]
Immobilized hIFNγ (μg/mL)	25	25	10	4	1	0.2	0.02
Wash times	5	10	10	10	10	10	10
Tween-20 in Wash buffer (%)	0.05	0.05	0.25	0.5	1	1	1

[a]Clones obtained after five rounds of selection are called PM series in clone list (Fig. 3).
[b]Clones obtained after seven rounds of selection are called JA series in clone list (Fig. 3).

plasmids with cloned DNA were transformed into *E. coli* BL21 (DE3). Individual clones producing various ABD-TolA proteins were grown from colonies randomly picked from an agar plate in 96 deep-well plates in 1 mL of Luria-Bertani (LB) medium with 60 μg/mL of kanamycin and 0.2 m*M* isopropyl-beta-D-thiogalactopyranoside (IPTG). After cultivation for 18 h at 37°C, the bacteria were pelleted by centrifugation at 3000*g* for 30 min, and the supernatant was discarded. A total of 250 μL of PBS containing 0.1% Tween-20 (PBST) and 200 μg/mL lysozyme was used to resuspend the pellet, and cells were lysed by three cycles of freezing at −80°C for 30 min followed by thawing in a water bath at 37°C for 30 min. The resulting suspensions were centrifuged at 3000*g* for 30 min, and 50 μL of supernatant from each well was applied to a PolySorp microtiter plate (NUNC) coated with hIFNγ at the concentration 5 μg/mL. Upon 1 h incubation at room temperature, the plate was washed with PBST five times, anti-His-tag antibody diluted (1:5000) in PBS with 3% BSA (PBSB) was added for 45 min, and the plate wells were washed repeatedly and developed in 0.1*M* citrate buffer, pH 5.0 containing 0.5 mg/mL *o*-phenylenediamine (OPD) and 0.01% H_2O_2 for 5 min. The colorimetric reaction was stopped by adding 100 μL 2*M* H_2SO_4 and absorbance at 492 nm was determined. Lysate containing wild-type (WT) version of ABD, ABD-WT-TolA fusion protein, was applied to HSA-coated wells to serve as positive control, whereas negative control background was determined in wells coated with 3% BSA. Identity of constructs yielding ABD variants binding to hIFNγ was determined by DNA sequencing.

Sequence analysis, clustering, and modeling of selected ABD variants

Multiple sequence alignment and construction of the similarity tree was performed using the ClustalW program.[39] The tree is presented as a phenogram rendered by the Phylodendron online service (http://iubio.bio.indiana.edu/treeapp). The homology modeling of selected ABD variants was performed using the Modeller program[40] based on the ABD_WT as a template. Resulting three-dimensional structures were refined by the FoldX program[41] and Stricher et al., (in preparation) and subjected to flexible side chain docking to the hIFNγ (3D structure taken from the PDB code 1FG9). The docking was performed using the ClusPro server.[42] For each selected ABD variant, we ran a short (2 ns) molecular dynamics (MD) simulation of the top 10 predicted structures of the complex using the Gromacs version 4 suite of programs.[43] The solute was put inside a periodic box of water and charge neutralizing ions with dimensions exceeding the size of the solute by 10 Å in each direction and simulated at constant 300 K and 1 atm conditions with cutoffs of 10 Å and 2 fs time step, using the FF03 force field[44] with the TIP3P explicit water solvation model. The snapshots of geometry (nonminimized, saved each 1 ps) from last 500 ps of each trajectory were used to calculate the averaged ΔG of binding within the FoldX force field approximation.

Production of ABD-TolA proteins

Two milliliters of overnight cultures of clones producing interferon binders were inoculated into 200 mL of LB medium containing 60 μg/mL kanamycin and grown for 4 h at 37°C, before 1 m*M* IPTG was added for additional 4 h. Cells were harvested by centrifugation at 4000*g*, pellets were resuspended in 25 mL of lysis buffer (50 m*M* NaH_2PO_4, 300 m*M* NaCl, 10 m*M* imidazole, pH 8.0), and cells were disrupted by ten 10 s ultrasound pulses at 27 W power output (Misonix S3000). The lysates were centrifuged for 20 min at 23,700*g*, applied to 1 mL Ni-NTA columns (Qiagen) equilibrated with lysis buffer, and the columns were washed with 20 mL of wash buffer (lysis buffer containing 20 m*M* imidazole). ABD-TolA fusion proteins were eluted with 5 mL of lysis buffer containing 250 m*M* imidazole. Typical yield of purified ABD-TolA protein produced by *E. coli* BL21 host cells in LB broth medium is more than 20 mg/L.

ELISA assay for binding to hIFNγ

Serially diluted purified ABD-TolA variants were applied to the Polysorp microtiter plate coated with 5 μg/mL hIFNγ, and the plate was incubated at RT for 1 h. The plate was washed five times with ice-cold PBST and monoclonal Anti-His_6-tag-horse radish peroxidase (HRP) conjugate solution in PBSB (dilution 1:5000) and OPD substrate were used to detect bound ABD-TolA proteins as above. The plots of absorbance at 492 nm versus ABD concentration were subjected to sigmoidal fitting using Origin software (OriginLab Corporation, USA) and apparent dissociation constants (K_d) were calculated.

Competition ELISA with synthetic ABD35

Polysorp 96-well plate (NUNC, Denmark) was coated with 100 μL coating buffer containing 10 μg/mL hIFNγ

(produced by Proteix, s.r.o., Czech Republic) and kept at 4°C overnight. The plate was washed with PBST (PBS with 0.05% Tween-20) pH 7.4, and blocking step was done using 300 µL 1% BSA in PBST followed by 2 h incubation at 37°C. The plate was then washed with PBST three times. Serially diluted synthetic ABD35 protein variant (46 residues, Institute of Organic Chemistry and Biochemistry ASCR, v.v.i., Prague, Czech Republic) was added into wells containing 100 n*M* solutions of individual ABD-TolA variants in 1% BSA/PBST. Following 2 h of co-incubation at room temperature, the plate was washed five times with PBST and 100 µL of 5000-fold diluted monoclonal anti-polyhistidine peroxidase conjugate was added into each well for 1 h, before the plate was washed three times with PBST and OPD solution was added. Reaction was stopped by 2*M* sulfuric acid and absorbance at 492 nm was measured.

Preparation of *in vivo* biotinylated hIFNγ

A DNA fragment encoding a 143 residue-long variant of hIFNγ with an N-terminal methionine residue and a C-terminal AviTag consensus sequence (GLNDIFEAQKIEWHE) was PCR-amplified using appropriate primers, cloned in the pET-28b vector, and used to transform *E. coli* BL21 (DE3) BirA cells. C-terminally biotinylated hIFNγ-AviTag protein was produced in *E. coli* cultures upon induction with 1 m*M* IPTG in the presence of 50 µ*M* D-biotin (Sigma-Aldrich), extracted from inclusion bodies with 8*M* urea in 50 m*M* Tris buffer (pH 7.4) and purified by chromatography on SP Sepharose pH 7.4 followed by Phenyl Sepharose CL-4B (Pharmacia) at pH 7.4. The eluted hIFNγ-AviTag protein was dialyzed into 50 m*M* ammonium acetate solution pH 5.0.

Preparation of *in vivo* biotinylated ABD variants

To express and produce ABD variants without TolA moiety, a 19 residue-long N-terminal *trp* leader sequence (MKAIFVLNAQHDEAVDAMD) was fused to the ABD scaffold sequence and a C-terminal AviTag biotinylation consensus sequence (GLNDIFEAQKIEWHE) was added. This yielded 82 amino acid residue-long ABD-AviTag constructs. These ABD-AviTag binders were produced as biotinylated proteins in *E. coli* BL21 (DE3) BirA strain, expressing the biotin ligase (BirA), as above and were extracted from inclusion bodies with solution of 50 m*M* Tris, 150 m*M* NaCl, 8*M* urea, pH = 8.0.

Production of soluble recombinant hIFNγ receptor 1 (hIFNγR1)

A codon-optimized synthetic gene encoding the mature 228 residue-long extracellular domain of hIFNγR1 with an N-terminal methionine residue and a C-terminal LEHHHHHH polyhistidine tag (237 residues in total, 27 kDa) was purchased from GenScript (USA). The soluble form of the receptor was produced in IPTG-induced *E. coli* SHuffle T7 Express cells (New England Biolabs, USA) at 16°C, and the protein was purified from cytoplasmic extracts using metallo-affinity chromatography on Ni-NTA agarose (Qiagen).

Binding specificity testing

Polysorp 96-well plate (NUNC, Denmark) was coated at 4°C overnight with 10 µg/mL of different target proteins (hIFNγ, Culture Filtrate Protein-10/Early Secreted Antigenic Target 6 complex, lysozyme, BSA, HSA) and human serum (1:10 dilution in coating buffer). The plate was washed with PBST (PBS + 0.05% Tween-20) pH 7.4, and blocked with 2% BSA in PBST for 1 h at 30°C. After washing, His_6-ABD-TolA proteins at indicated concentrations in PBST with 2% BSA were added. Binding of His_6-ABD-TolA variants was detected by Anti-His-tag monoclonal antibody conjugated with HRP at 1:4000.

Chemical biotinylation of ABD-TolA proteins

Before immobilization on the biosensor chip for surface plasmon resonance (SPR) measurements, C-terminal carboxyl groups of ABD-TolA proteins were labeled with biotin hydrazide. Purified ABD-TolA proteins were dialyzed against the reaction buffer (10 m*M* 2-(N-morpholino)ethanesulfonic acid (MES) pH 4.8). Then, 2.5 µL of 5 m*M* biotin hydrazide (Sigma-Aldrich) in dry dimethyl sulphoxide and 1.25 µL 50 m*M* 1-ethyl-3-(3-dimethylaminopropyl)carbodiimide hydrochloride (EDC) (Sigma-Aldrich) in reaction buffer were added per mg of the protein, mixed, and incubated for 2 h. To remove nonreacted biotin hydrazide, EDC, and the precipitate occasionally forming during the reaction (cross-linked proteins), the solution was centrifuged for 2 min at 5000 RPM and the supernatant was dialyzed against SPR running buffer (10 m*M* HEPES 7.4).

Preparation of the SPR biosensor

All modification steps were performed sequentially on an SPR chip inserted in the microfluidic block of a SensiQ instrument (ICX Nomadics, USA) with on-line control of the degree of modification [resonance unit (RU)]. The temperature was set to 25°C and flow rate to 10 µL/min. After thermal equilibration of the chip (2 h), the carboxyl groups of the chip (COOH-2, ICX Nomadics) were activated in both reference and measurement channels with injection of 200 µL of freshly prepared mixture of 0.4*M* EDC and 0.1*M* N-hydroxysuccinimide (NHS) (MES buffer pH 6.0). Biotin hydrazide was next covalently coupled to surface of the working channel in 1.25 m*M* MES pH 4.8 (200 µL injection). Free NHS-ester groups were deactivated by injecting 200 µL of 1*M* ethanolamine-hydrochloride pH 8.5 into both channels.

Then, the flow rate was reduced to 5 μL/min, and the working channel surface was coated with avidin (50 μL injection, 100 n*M* in running buffer). Finally, 100 μL of biotinylated ABD-TolA variants (2.5 μg/mL, running buffer) was injected and bound to the surface (∼ 100 RU) due to the avidin-biotin interaction.

SPR analysis with immobilized ABD-TolA

The flow rate (25 μL/min) and temperature (25°C) were held constant during the SPR experiments. hIFNγ stock solution (8.2 μ*M* in running buffer) was prepared from a frozen aliquot in 50 m*M* acetate buffer pH 5.0. Serial dilutions (25–200 n*M*) of hIFNγ as analyte were prepared and sampled into both working and reference channels. The assay template was set as follows: association of the hIFNγ with the immobilized ABD-TolA (180 s, 75 μL of the hIFNγ), intermission time for observing the dissociation (running buffer flow, 360 s), and finally, the regeneration of the sensor surface (25 μL solution of 0.05% SDS and 0.15 m*M* HCl, 600 s running buffer flow). The last step allowed to recover the initial baseline and to start another assay cycle. Reference channel was used for real-time reference curve subtraction. Blank buffer injections were used to allow double referencing of the data set. Data processing and kinetic model fitting were performed using Qdat, derived from Scrubber2 and developed by BioLogic Software (Australia). A 1:1 fitting model without mass transport limitations was chosen for calculation of K_d using a set of 5 SPR binding curves. All parameters (k_{on}, k_{off}) except for R_{max} were fitted globally. The obtained residual standard deviations were lower than 5% of the maximum experimental response. For the validation of the curves and parameter values, the residual plot was inspected for nonrandom distribution.

SPR analysis with free ABD-TolA

SPR measurements of free ABD-TolA proteins were carried out using custom SPR biosensors (Institute of Photonics and Electronics AS CR, v.v.i., Prague, Czech Republic) with four independent sensing spots.[45] The SPR sensor output is stated in nanometers (nm) and describes the spectral shift of SPR. The response in nm can be easily transformed to units used by BIACORE instruments using the calibration equation: 1 nm = 150 RU. Briefly, recombinant streptavidin was covalently linked to sensor chip surface as described[46] and used to capture the biotinylated hIFNγ target. To suppress nonspecific adsorption, the chip surface was blocked for 10 min with a solution of 500 μg/mL BSA in SA buffer. Attachment of biotinylated hIFNγ was performed in SA buffer (10 m*M* sodium acetate, pH 5 at 25°C). Once a stable baseline was reached, solution of hIFNγ was flowed across the sensing surface for 10 min. This step was followed by washing of the sensor surface with SA buffer. Running buffer (10 m*M* HEPES, 150 m*M* NaCl, 50 μ*M* EDTA, 0.005% Surfactant P20, pH 7.4, 25°C) was injected into the flow-cell until the baseline became stable. The solution of particular ABD-TolA variants at concentrations ranging from 20 to 500 nM were injected into the measuring (+hIFNγ) and reference (−hIFNγ) channels. After 5 min incubation, ABD-TolA solution was replaced with running buffer, and the dissociation was monitored for at least 15 min. Each concentration was measured on at least two different SPR chips. Reference-compensated sensor responses to at least three concentrations were fitted with Langmuir model implemented in BiaEvaluation software, taking mass transport into account. All the measurements were performed at 25°C and flow-rate of 30 μL/min.

RESULTS

Computational analysis of mutability of the GA module

To generate a library of the ABD scaffolds, we identified ABD residues suitable for randomization, the substitution of which was unlikely to affect the structure and stability of ABD. Inspection of the structure of the HSA complex with ALB8-GA protein revealed that residues from the conserved consensus sequence of the GA module family (helices 2 and 3 with residues 19–27 and 31–44, respectively) are in contact (i.e., within less than 4 Å) with the HSA chain.[27] It was, hence, plausible to assume that the conserved residues not participating in HSA binding (i.e., residues L1, A4, K5, A8, E11, L12, D19, I25, N26, V31, and L42) were structurally important and must not be mutated to preserve scaffold stability. The consensus analysis, however, did not allow assessing the structural importance of residues that were in contact with HSA. These, in turn, needed to be randomized to eliminate HSA binding and generate novel binding specificities to unrelated targets.

To this end, the solved NMR structure of ABD (ABD-WT) was analyzed using the IEM method,[30] to computationally assess the overall stability changes of the scaffold following substitution of individual amino acid residues. Contribution of each residue to stabilization of the ABD structure was calculated as the sum of its pair-wise interaction energies (E_{int}) with all other ABD residues except sequence neighbors. Residues with the lowest (most negative) value of total interaction energy were then taken as key stabilizing residues of the structure. At the same time, the key residues were also characterized by a high number of stabilizing interactions ($E_{int} < -0.5$ kcal/mol).

As shown in Figure 2(a), the residues revealed by IEM as bringing the largest stabilization to the structure were, in the order of decreasing contribution, L12 (−17.7 kcal/mol), K5 (−17.0 kcal/mol), I25 (−16.7 kcal/mol), R10 (−15.3 kcal/mol), N9 (−15.2 kcal/mol), A8 (−14.5 kcal/

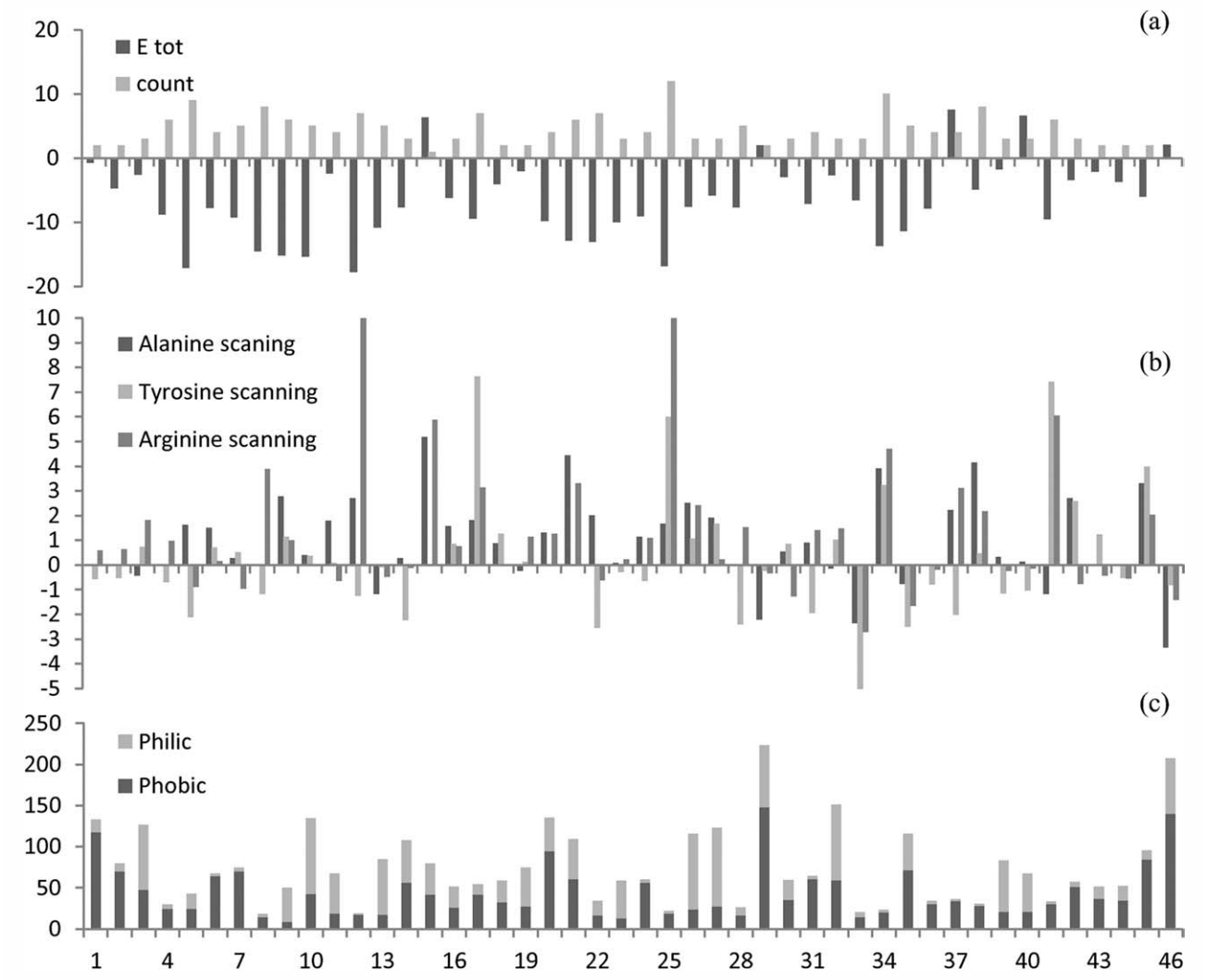

Figure 2

Computational analysis of ABD mutability. (**a**) Total interaction energies (E_{tot} in kcal/mol) for individual amino acid residues of the ABD structure (black) and the number of stabilizing interactions ($E_{int} < -0.5$ kcal/mol) for each residue (gray). (**b**) ABD stability change ($\Delta\Delta G$, in kcal/mol) upon *in silico* alanine, tyrosine and arginine scanning. (**c**) SASA of individual ABD residues. The size of the bar denotes the total SASA of the residue, the proportion of hydrophilic SASA and hydrophobic SASA denoted in gray and black color, respectively. Calculation was done using POPS server.[34,35]

mol), V34 (−13.6 kcal/mol), respectively (E_{tot} in parenthesis). Interestingly, not all of these key residues were nonpolar residues forming the hydrophobic core, for example, with small SASA. Despite their large SASA [c.f. Fig. 2(c)], three out of seven of the key residues found to substantially contribute to ABD stability were, indeed, the polar and charged residues K5, N9, and R10. Importantly, these were all located at the surface of helix 1, and none of the residues predicted to form the stabilizing framework was located in helices 2 and 3, which are involved in binding of HSA. These results suggested that randomization of helices 2 and 3 would not only yield loss of HSA binding but may also have little or no impact on stability of the ABD scaffold.

Destabilization effects caused by residue substitutions were first assessed by *in silico* scanning mutagenesis of the ABD surface formed by helices 2 and 3 [Fig. 2(b)]. Besides alanine scanning, also tyrosine and arginine residue scanning was performed to assess the impact of insertion of the bulkier residues that are frequently found at protein–protein interfaces.[47,48] The predicted changes in protein stability induced by individual substitutions ($\Delta\Delta G$) were calculated using the Eris server[36] and advantage was taken of the capacity of Eris to model backbone flexibility and mutation-induced backbone conformational changes. This approach was previously shown to be particularly important for $\Delta\Delta G$ estimation of small-to-large mutations, thus allowing to increase the accuracy of prediction and yield-

ing significant correlation with the experimental data.[49] As shown in Figure 2(b), in the 26 residue-long segment comprising helices 2 and 3 (positions 16–45), the Eris scanning protocol identified the residues V17, Y21, I25, V34, and I41 as nonmutable. With the exception of residue Y21, these residues mostly appear to be nonpolar and buried in the hydrophobic core of ABD. In combination with the assessment of SASA [Fig. 2(c)], this computational analysis allowed to chose 11 surface residues of ABD, the randomization of which was predicted to have the least impact on stability of the ABD scaffold (e.g., Y20, L24, N27, K29, T30, E32, G33, A36, L37, E40, and A44).

Ribosome display selection of hIFNγ binders

To screen for hIFNγ binders, a synthetic oligonucleotide library was designed in NNK code with 11 codon positions randomized, yielding a theoretical complexity of 32^{11} codons ($= 3.6 \times 10^{16}$). Taking into account, the redundancy of the genetic code, where the same amino acid residue can be encoded by up to six synonymous codons, randomization of 11 codons of the the ABD encoding sequence was expected to give rise to $\sim 2 \times 10^{14}$ (i.e., 20^{11}) ABD variants. A library of 10^{14} oligonucleotide molecules was synthesized, bearing randomized codons at selected position of the ABD gene and $\sim 10^{13}$ annealed double stranded oligonucleotide molecules (25 pmol) were used per reaction to assemble a library of genes encoding randomized ABD-*tolA* fusion constructs by successive rounds of PCR-mediated assembly. The obtained DNA template pool was subjected to *in vitro* transcription and used for *in vitro* translation, yielding formation of ternary complexes of ribosomes with attached nascent ABD-TolA fusions proteins. These were selected for binding to immobilized hIFNγ in hIFNγ-coated microtiter plates, with successively decreasing the coated target protein (hIFNγ) concentration and increasing the stringency of washing after each selection cycle (increasing the number of wash cycles and the detergent concentration).

In the first selection campaign, consisting of five rounds of ribosome display, a collection of total 32 of clones [Petr Maly (PM) series] was retained for sequencing (Fig. 3) and 13 of them were selected for more detailed characterization.

To increase the probability of finding strong hIFNγ binders, the selection campaign was repeated, increasing the number of ribosome display selection rounds to seven and starting from an independently constructed library. Here, 321 clones were picked in total and analyzed by ELISA for production of hIFNγ binders (data not shown). In this collection [Jawid Ahmad (JA) series], 15 of ABD-TolA fusion constructs exhibiting the best binding properties were selected for sequencing (Fig. 3) and further characterization.

Sequence analysis and clustering

Sequences of 47 construct (32 from PM series and 15 from JA series), exhibiting hIFNγ binding in ELISA screening, were determined and compared. Only about 1.3% of all detected changes were PCR-introduced errors, with only five codon-changing base substitutions (5 of 47 × 19 positions, 0.56%) found in the first 19 codon segment excluded from randomization. In turn, a total of 17 unintended mutations (3 deletions and 14 substitutions) were found within the 16 nonrandomized codons encoding helices 2 and 3 of ABD (Fig. 3). This corresponded to an average error frequency of 2.26% (17 of 47 × 16 positions). As these mutations were mostly adjacent to randomized codons, such bias (4.03-fold) may indicate a positive selection during ribosome display for unintended mutations that contributed to hIFNγ binding capacity of the selected ligands.

Further, the relative average occurrence of individual amino acid residues at the 11 randomized positions was compared for the PM and JA clone series. For most of the amino acid residues, a roughly equal frequency of occurrence at the randomized positions was observed in both clone series. However, a noteworthy increase of arginine (3.0×), tryptophane (2.4×), and phenylalanine (2.4×) occurrence at randomized positions was observed within clones of the PM series, as compared with clones of the JA series. In turn, the JA series clones were statistically enriched for proline (3.7×), glutamine (6.4×), and aspartate (10.6×) residues at the randomized positions. Further sequence differences between clones from the two series could also be documented by the increased occurrence of frequently represented residues, where the overall content of arginine + tryptophane residues in the PM series was 22.3%, compared with 10.3% in the JA series. In the case of proline + serine residues, the values of 8.5% and 22.4% were, respectively, found for proteins selected in the two series. This suggests that sequence characteristics can be derived for clones originating from either of the two series. This indicates that enhanced stringency during selection of the JA clone series (see Table I) may have biased the preference for certain amino acid residues in the ligands that were retrieved by the ribosome display.

To further investigate the sequence similarity among all analyzed ABD variants, clustering using ClustalW program was performed. On the basis of a similarity tree, subgroups of ABD variants with highest similarity were identified (Fig. 3). Although the overall similarity calculated for all 47 clones was found to be on average at an 80.22% level, it varied between 81.52 and 86.74% between group members. Nevertheless, a general sequence consensus representing a shared hIFNγ-binding motif in the obtained ABD variants and their subgroups could not be identified. This suggests that the characterized ABD variants may bind hIFNγ in several modes.

Affinity and specificity of ABD-derived ligands

Whole cell lysates, controlled for ABD content by Western blots, were used to define an initial set of 28

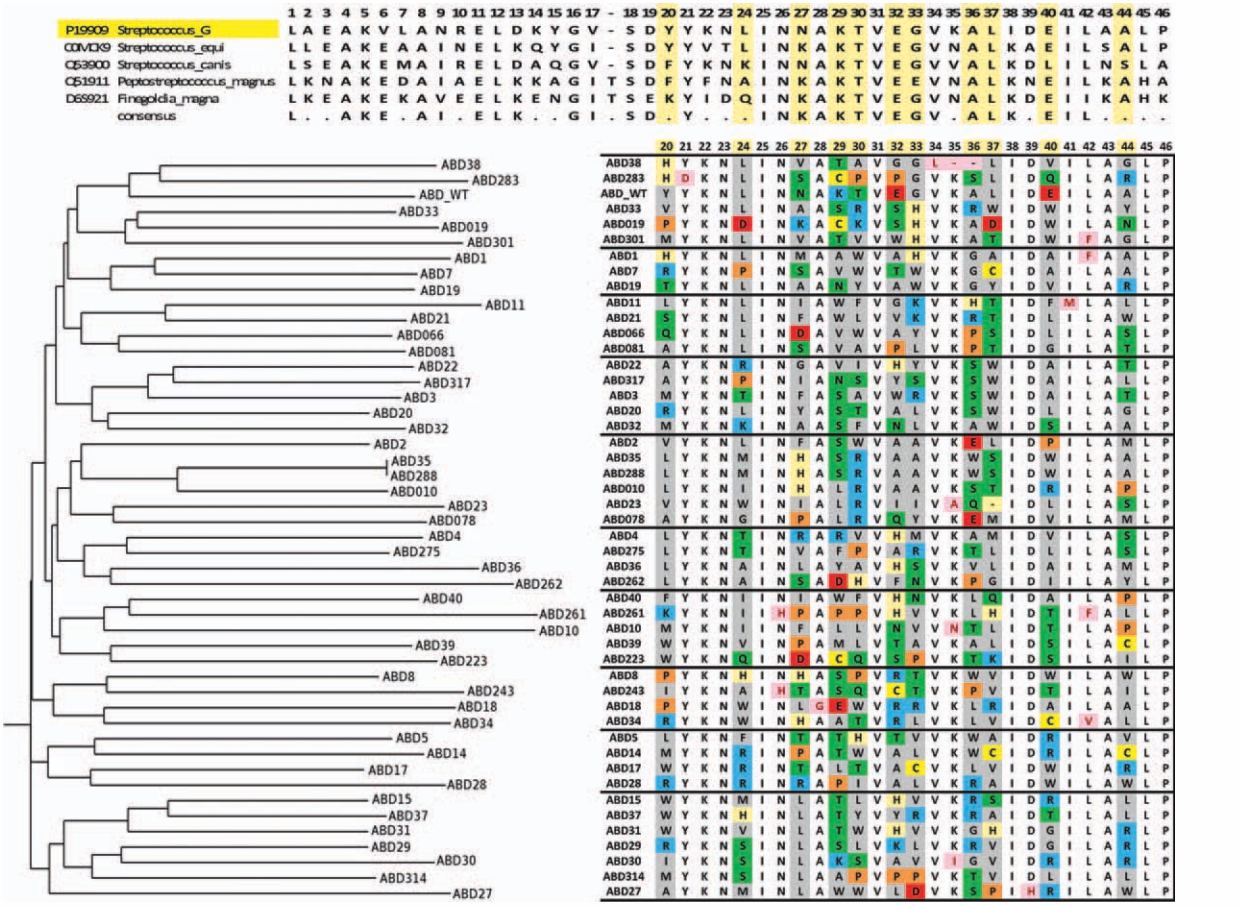

Figure 3

Similarity tree of ABD variants binding hIFNγ. ABD of streptococcal protein G (highlighted in yellow, G148_GA3) was aligned with homologous protein sequences available in the UniProt database (top) and the randomized portions of sequenced ABD variants selected in ribosome display for hIFNγ binding (lower part). Positions of 11 randomized residues are indicated using a color code, according to residue type. Pink boxes indicate unintended mutations within the randomized ABD segment corresponding to residues 20–46. In the nonrandomized N-terminal part of ABD (residues 1–19, not shown), 5 unintended substitutions were present (E3G, L1S, R10K, K5E, and N9K in ABD10, 14, 28, 36, and 262, respectively). Multiple alignment and similarity tree construction was performed in ClustalW.[39] Clones numbered ABD010, ABD019, ABD066, ABD078, ABD081, ABD223, ABD243, ABD261, ABD262, ABD275, ABD283, ABD288, ABD301, ABD314, and ABD317 represent JA series, all other clones belong to PM series, ABD_WT indicates sequence of parental nonmutated ABD.

best binders within the PM and JA clone series. Constructs yielding the highest apparent affinity for hIFNγ in ELISA were chosen for purification of the corresponding His_6-ABD-TolA fusion proteins, as documented in Figure 4. These 363 residues-long fusion proteins consisted of a twelve residue-long N-terminal 6×His tag fused to a 46 residue-long ABD scaffold moiety and a 305 residue-long TolA tail, making for a calculated molecular mass of 36.3 kDa on average. ELISA was used for preliminary assessment of binding properties of 11 purified His_6-ABD-TolA constructs and the affinity of best binders for hIFNγ was determined by SPR biosensor measurements for six best binders.

In the first setup, ABD-TolA variants were biotinylated *in vitro*, immobilized onto avidin-coated SPR sensors and hIFNγ was circulated at different concentrations over the chip surface. In the reversed setup, *in vivo* biotinylated hIFNγ was immobilized and binding of circulating His_6-ABD-TolA proteins was measured. As documented by representative binding curves for the ABD29-TolA and ABD35-TolA variants in Figure 5(a,b) and summarized in Table II, the six characterized ABD-TolA variants exhibited a K_d value for hIFNγ in the nanomolar range.

To verify that presence of the C-terminal TolA spacer in the His_6-ABD-TolA proteins did not interfere with binding of the ligand to hIFNγ, SPR measurements were performed with a chemically synthesized ABD35 binder variant comprising only the 46 residues of the scaffold. A slightly lower affinity of the synthetic ABD35 toward immobilized biotinylated hIFNγ ($K_d \sim 19$ n*M*) was found than that observed for the His_6-ABD35-TolA-fusion protein ($K_d \sim 10$ n*M*). This may suggest that fusion to the

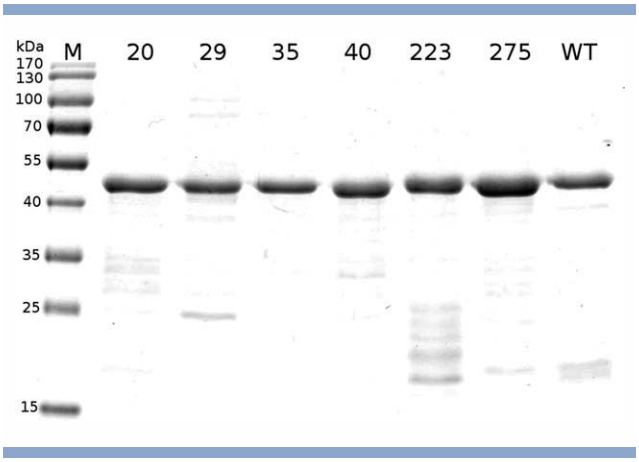

Figure 4

SDS-PAGE electrophoresis of ABD-TolA variants. The ABD-TolA fusion proteins with N-terminal polyhistidine tag were purified from *E. coli* cell lysates on Ni-NTA and separated on 12.5% polyacrylamide gel stained by Coomassie blue.

Table II

Affinity of Selected ABD-TolA Variants Binding to Recombinant hIFNγ Measured Using SPR

ABD variant	K_d (n*M*) Immobilized biotinylated ABD clones	K_d (n*M*) Immobilized biotinylated hIFNγ
35	0.2	10.0 ± 0.2
275	0.8	8.4 ± 0.6
29	1.5	1.8 ± 0.2
223	2.4	4.6 ± 0.4
20	3.5	2.7 ± 0.3
40	6.5	9.2 ± 0.7

TolA spacer may stabilize the structure of ABD. Alternatively, the orientation of surface-bound His_6-ABD35-TolA-fusion protein and bound hIFNγ may allow for avidity effects, that is, the hIFNγ dimer can bind more than one ABD protein. These effects, however, cannot occur in the reverse setting, where the ABD proteins are in solution and hIFNγ molecules are immobilized on the surface. Moreover, the affinities of the best His_6-ABD-TolA constructs for hIFNγ compared well to the affinity of recombinant version of the extracellular domain of hIFNγ receptor 1. This exhibited a K_d value of ∼ 1.7 n*M*, in good agreement with published values ranging from of 1.4 to 2.0 n*M*.[50] It can, hence, be concluded that the recombinant ligands derived from the engineered ABD scaffolds exhibited a similar affinity for hIFNγ as its natural receptor.

To investigate the selectivity of hIFNγ binding, ELISA experiments were performed on microplates coated with HSA, complete human serum or with several unrelated purified proteins (hen egg lysozyme or *Mycobacterium tuberculosis* ESAT-6 and CFP-10 antigens). As documented in Figure 6(a), the tested ABD-TolA constructs bound hIFNγ with a high selectivity and exhibited a minimal binding to HSA or BSA, in contrast to wild type His_6-ABD-TolA that bound HSA with high affinity [Fig. 6(b)]. The randomization of residues from the F23 surface of ABD [cf. Fig. 1(b)], hence, lead to a sharp loss of binding capacity for HSA and generated a new binding specificity for hIFNγ. The WT ABD-TolA construct, used as control, exhibited some background binding to

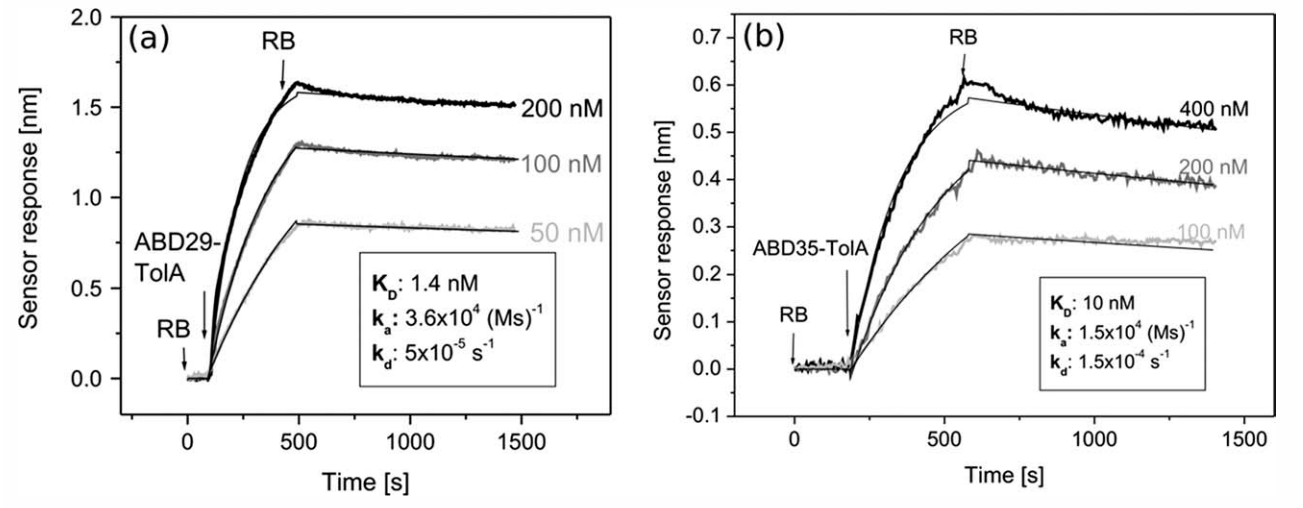

Figure 5

SPR analysis of binding of two ABD variants to immobilized hIFNγ target. C-terminally biotinylated hIFNγ was immobilized on streptavidin-coated biosensor chip and (**a**) ABD29-TolA or (**b**) ABD35-TolA proteins were flowed over chip surface in running buffer (RB). The recorded biosensor response was fitted with a 1:1 model considering mass transport limitations.

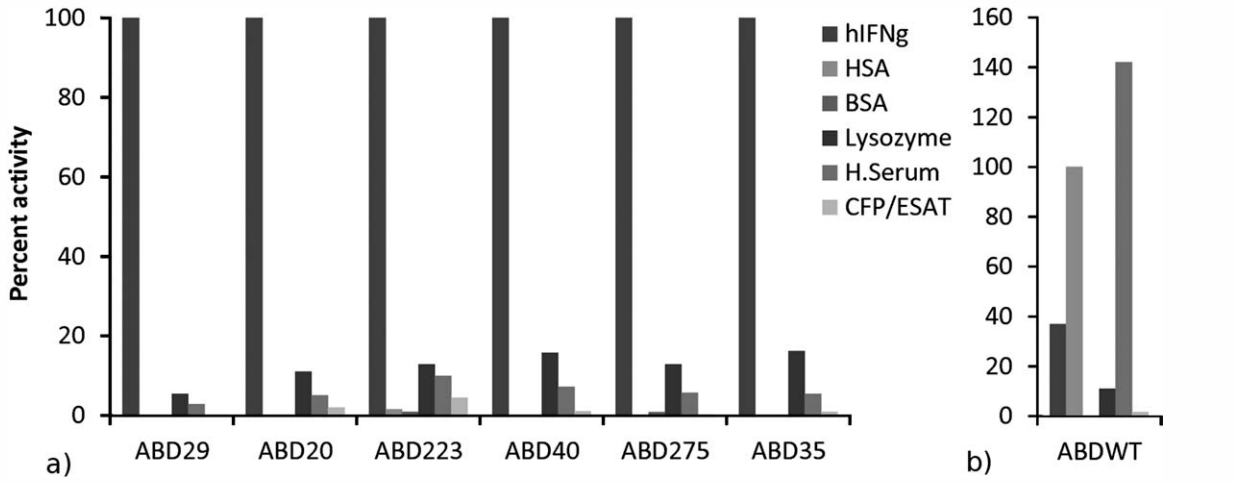

Figure 6

Binding specificity of ABD variants. Binding of purified ABD-TolA proteins to indicate target proteins coated on microplate wells was determined by ELISA. Average values from three independent experiments are shown. (**a**) Percentage of binding of indicated ABD-TolA proteins to various targets. Binding to hIFNγ was taken as 100%. HSA, human serum albumin; CFP/ESAT, culture filtrate protein-10/early secreted antigenic target 6 complex. (**b**) Binding of the initial (WT) ABD-TolA construct molecule to the coated proteins. Binding to purified human serum albumin (natural ABD target) was taken as 100%.

the IFNγ target. This might reflect an unspecific interaction of the TolA moiety with IFNγ as well as some initial capacity of intact WT ABD to bind IFNγ with a low affinity, which upon randomization and selection was enhanced by several orders of magnitude.

ABD variants all bind the same hIFNγ surface

We used molecular modeling approaches to explore the binding regions possibly recognized on the surface of hIFNγ by the engineered ABD scaffolds. To obtain predicted structures of the selected ABD variants, homology modeling with ABD was performed using wild type structure as a template, followed by a side-chain relaxation. Binding positions were predicted based on docking of the modeled ABD variant structures onto the known hIFNγ structure and a set of 10 most probable arrangements of the complex with each variant was identified. This was subjected to prediction of binding affinity (ΔG). Analysis of the best scoring binding modes of the different ABD variant predicted that all of them are likely to occupy a common binding region on hIFNγ that was different from the binding site recognized by the hIFNγR1 (Fig. 7). To investigate whether the individual ABD variants recognized identical or overlapping epitopes on the surface of the hIFNγ, their competition for hIFNγ binding was examined. WT-ABD-TolA protein was used as a noncompeting control, the competition for hIFNγ binding between synthetic ABD35 and its His_6ABD35-TolA variant was used as a positive control. As indeed documented in Figure 8, at increased concentrations, the synthetic ABD35 protein out-competed all tested His_6-ABD-TolA variants from binding to hIFNγ.

To further investigate whether individual ABD-TolA proteins competed with each other for hIFNγ binding, competition of pairs of unlabeled and biotinylated His_6-

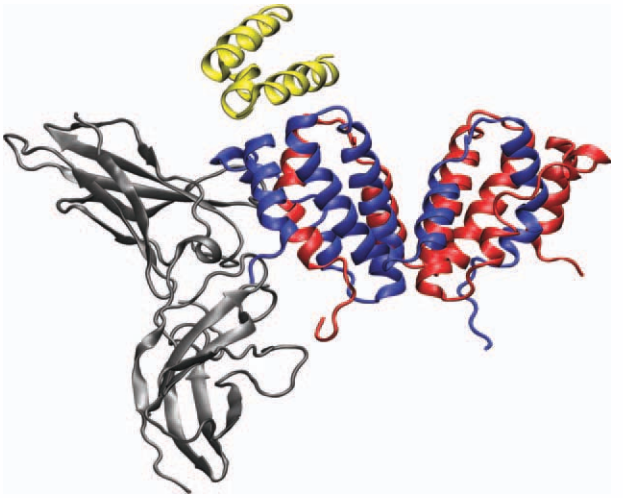

Figure 7

Model of ABD scaffold interaction with hIFNγ. Visualization of the predicted ABD binding site on hIFNγ. Individual ABD variant sequences were modeled on the template of the known ABD structure (PDB code 1GJT, residues 20–65) and docked onto the hIFNγ homodimer (PDB 1FG9) using ClusPro. The structure of hIFNγR1 (PDB 1FG9) was included into the model of the ABD-hIFNγ complex to highlight its different binding site.

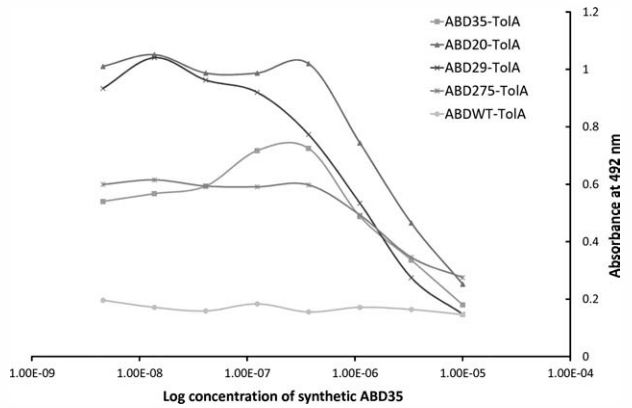

Figure 8

Different ABD-TolA proteins compete for binding to the same surface on hIFNγ. Synthetic ABD35 protein was serially diluted into microplate wells and allowed to compete for binding to coated hIFNγ in the presence of indicated His_6-ABD–TolA proteins (100 n*M*). The level of binding in the absence of competitor differs for individual ABD variants according to differences in affinity for hIFNγ (c.f. Table II).

ABD-TolA ligands was assessed. Here again, the results suggested that all tested ABD-derived ligands competed for binding to the same or overlapping binding site(s) on hIFNγ (data not shown).

To corroborate these results, SPR biosensor experiments were performed in which binding of synthetic ABD35 protein to immobilized hIFNγ-biotin was assessed following loading to 75% of maximal saturation and incomplete dissociation of the ABD35-TolA protein. A clear decrease of the sensor response to subsequent loading of synthetic ABD35 was observed, as compared with control channel to which only synthetic ABD35 was loaded (data not shown here). Moreover, competition for the binding to hIFNγ-biotin between the His_6-ABD20-TolA and His_6-ABD35-TolA proteins was also observed, as documented in Figure 9(a). In this experiment, the sensor with the immobilized hIFNγ molecules was preincubated with ABD35-TolA. At the end of the injection, the amount of bound ABD35-TolA reached ~ 80% of the saturation level (the saturation value was estimated from the fit of the data with Langmuir model using BiaEvaluation software). Because of the gradual dissociation of the ABD35-TolA, the saturation was about 65% of the maximum, just before the injection of the second ABD-TolA. A notable decrease in ABD20-TolA binding to the immobilized hIFNγ, compared with the binding to immobilized hIFNγ without the ABD35-TolA, was then observed.

To rule out the influence of steric hindrance due to the 305 residue-long TolA tail, competition experiments were also performed with ABD-AviTag proteins, which contained ABD extended only by a short 17-amino-acid long tail. As shown in Figure 9(b), significantly lower binding of ABD275-AviTag to immobilized hIFNγ was observed when the sensor was preincubated with ABD20-AviTag. This further supported the conclusion that the best hIFNγ binders derived from ABD recognize the same binding region on hIFNγ.

ABD variants bind to a different site than hIFNγ receptor 1

To examine the computational prediction that ABD scaffolds bind to a different site than the hIFNγ receptor

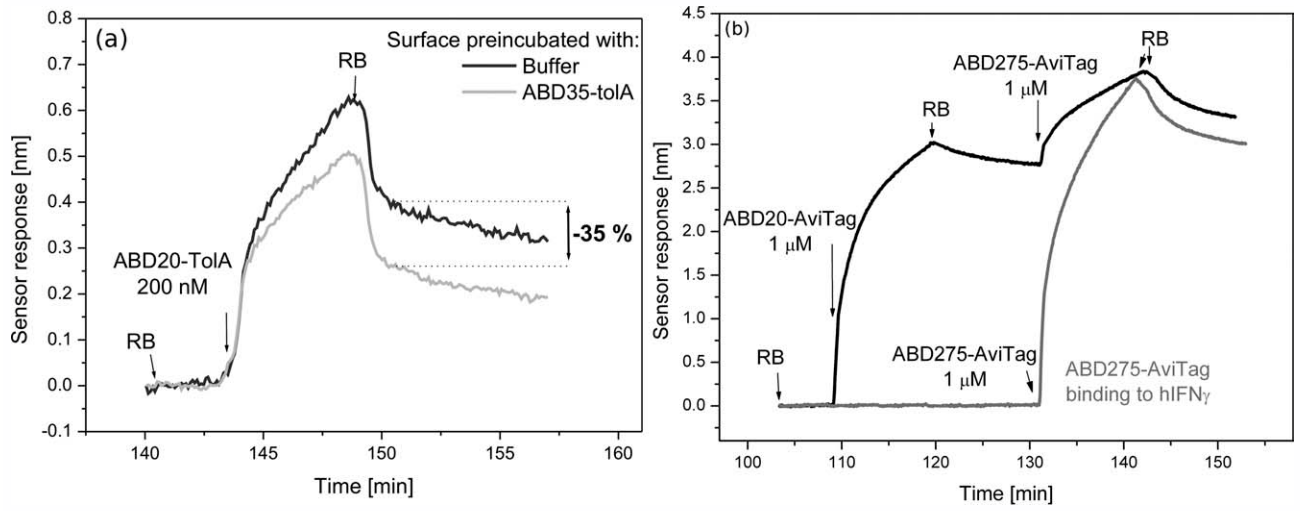

Figure 9

SPR analysis of competition for hIFNγ binding between selected ABD variants. (**a**) Sensor response to 200 n*M* ABD20-TolA binding to the immobilized hIFNγ that was preincubated with 800 n*M* ABD35-TolA and washed for 5 min. (**b**) Comparison of the kinetic curves for ABD275-AviTag binding to the immobilized hIFNγ upon preincubation with ABD20-AviTag (black line) and without the preincubation (gray line).

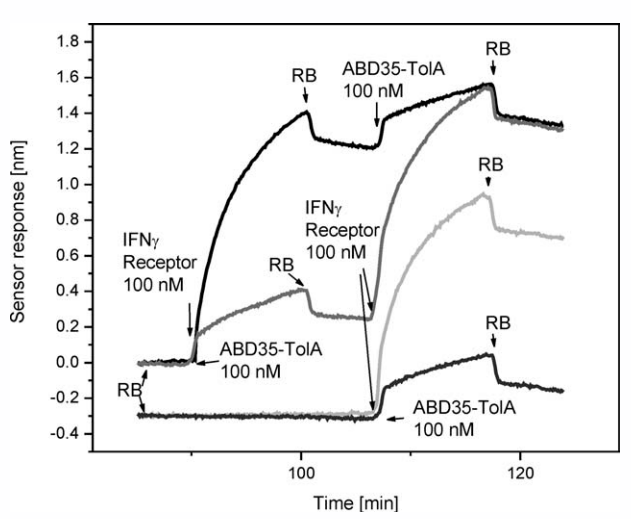

Figure 10

IFNγ receptor 1 and ABD35 ligand do not compete for binding to immobilized hIFNγ. Response of hIFNγ-coated SPR sensor to sequential binding of 100 n*M* ABD35-TolA and hIFNγ receptor 1 proteins (upper two lines), as compared with binding of the 100 n*M* proteins alone (lower two lines with lower offset). Arrows indicate the point at which indicated solutions were injected.

1 (hIFNγR1), competition between ABD35-TolA and the extracellular domain of hIFNγR1 was assessed. The SPR sensor was functionalized with biotinylated hIFNγ (as above), loaded for 10 min with 100 n*M* solution of hIFNγR1 protein, washed with running buffer, and exposed for 10 min to circulating ABD35-TolA protein at 100 n*M* concentration. The surface coverage with the hIFNγR1 reached about 90% of accessible binding sites, as estimated from the fit of the sensor response with Langmuir model. In the second channel, the order of interaction steps was reversed, starting with ABD35-TolA binding, followed by hIFNγR1 injection. Binding of hIFNγR1 and ABD35-TolA individually to immobilized hIFNγ was monitored in two other control channels. As shown in Figure 10, indeed, the order of the incubation steps had no influence on the final level of sensor response. Furthermore, no difference in the levels of response to subsequent binding of ABD35-TolA, or of hIFNγR1 was observed on sensors preloaded with the other protein. It can, hence, be concluded that hIFNγR1 and ABD35-TolA proteins bind to different sites on hIFNγ.

DISCUSSION

Construction of novel binders using a three-helix bundle scaffold has been already well documented in affibody molecules,[12,51] where randomization of 13 of total 58 amino acids immunoglobulin-binding domain of *Staphylococcus aureus* Protein A served as a powerful approach for the selection of high-affinity binders to several proteins, such as protein human factor VIII,[52] or recently ErbB3.[53] These novel binders lacking disulphide bonds exhibit several beneficial properties such as efficient refolding ability and high protein stability. Thus, the ABD scaffold represents another smaller three-helical alternative to affibodies.

Besides using hIFNγ as a model target for testing of the potential of the ABD scaffold to yield high affinity ligand, there was also a practical motivation to the present work. Selecting small scaffold binders for hIFNγ was aimed to generate high affinity ligands for applications in which antibodies fail, such as biosensors, where high shearing forces, pH changes, and reducing or denaturing conditions during sensor stripping, lead to loss of antibody functionality, whereas small scaffolds can easily refold to a functional state. In particular, the ABD ligands are aimed for use in biosensor detection of hIFNγ released upon specific antigenic stimulation of T lymphocytes in whole blood for detection of latent tuberculosis.

The results presented here document the usefulness of a semirational approach to design of artificial binding proteins (recombinant ligands) for a given target. Starting from a stable protein scaffold of only 46 residues, we performed the computational analysis of its structure and binding properties, in order to identify residues suitable for randomization for the purpose of generating a combinatorial library of protein scaffolds. This approach enabled us to restrict the need for randomization to only 11 positions of the ABD scaffold, where permutation of amino acid residues at 11 positions within a protein still yields $\sim 2 \times 10^{14}$ possible protein variants.

Moreover, attention was paid to pick for randomization the residues that were known to be involved in HSA binding. This allowed to ablate the natural binding affinity of ABD for HSA and to replace it with a newly engineered binding capacity for hIFNγ. Subsequent selection of binders using ribosome display allowed retrieving of ABD scaffolds that bound hIFNγ with a nanomolar affinity. This raises a question whether selection conditions can be optimized for any chosen target and how many selection rounds are sufficient for obtaining of ABD-derived binders with highest possible affinity from within a combinatorial scaffold library. Theoretically, the more selection steps during ribosome display are used, the higher the probability of enriching and selecting the best binders. With this assumption in mind, we performed two screening protocols with five or seven rounds of selection, respectively. The only difference between steps 5 and 7 was the concentration of the hIFNγ target that was decreased by a factor of 50 (Table I). Yet, changes in the statistical representation of certain residues selected at randomized positions in the two binder collections were observed, with no clear correlation to the experimentally determined levels of binding affinity for hIFNγ

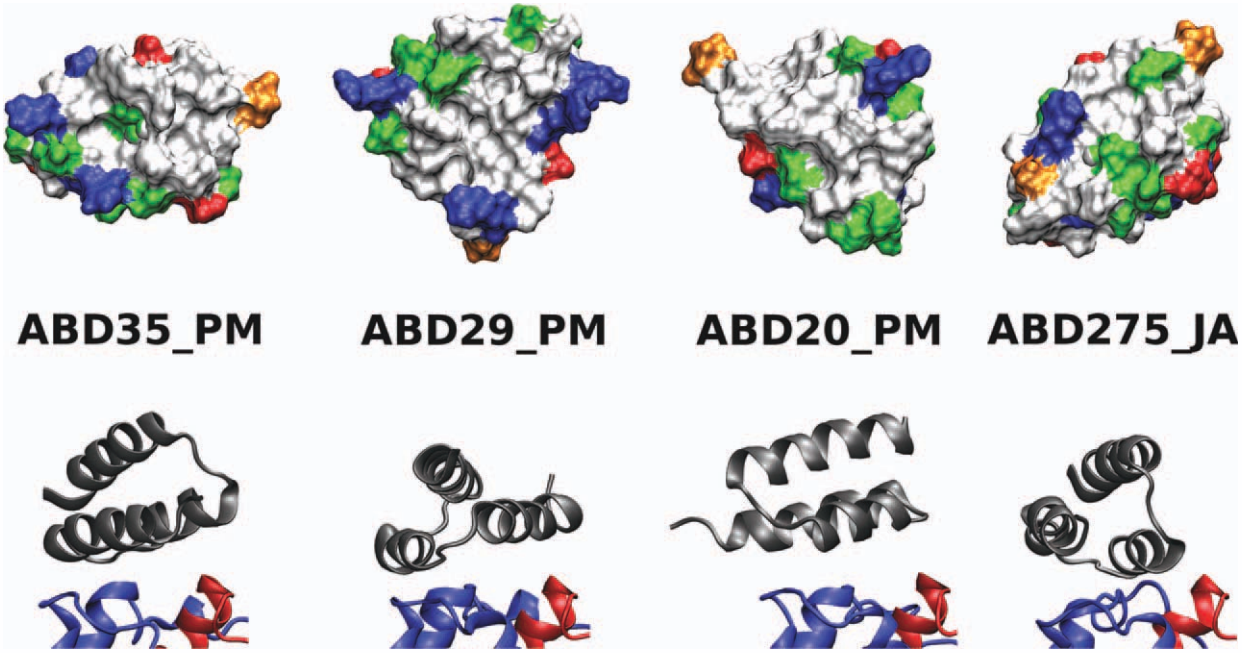

Figure 11

Predicted binding surfaces of indicated ABD variants (top) and their predicted modes of interaction with hIFNγ (bottom). Amino acid residues are color-coded as in Figure 3: gray, hydrophobic; green, polar; red, anionic; blue, cationic. Proline residue is given in orange. Orientation of a particular ABD binder is depicted with respect to the same hIFNγ reference position (blue-red cartoon representation).

being noticeable. In both selection series, the best obtained constructs exhibited binding affinities in the nanomolar range. In each round of ribosome display selection, however, the composition of the ligand pool and the complexity of retained binder library appeared to evolve according to increasingly stringent conditions. These appeared to result in changes in statistical representation of types of ABD variants in the pool. In the first rounds of *in vitro* selection, the ABD variants were likely sorted according to their affinity for the target. In contrast, the hIFNγ binders retained after the final rounds of ribosome display exhibited a similar level of binding affinity. These were likely selected in an affinity-independent manner. Nevertheless, two clones of identical sequence (ABD35 vs. ABD288) were found among the best hIFNγ binders obtained in two independent selection campaigns. This indicates that under the used conditions the function-directed statistical enrichment was sufficient and reached a plateau.

The affinity constants determined by SPR for ABD variants obtained in the two experimental setups revealed that the best hIFNγ binders derived from ABD exhibited K_d values in the nanomolar range. Most clones exhibited, indeed, rather similar binding affinities to immobilized or free hIFNγ target. However, the ABD35 and ABD275 variants demonstrated a substantial difference in target binding in the two SPR setups. Sub-nanomolar K_d values for binding of free hIFNγ from solution were observed with the biotinylated ABD35-TolA and ABD275-TolA variants immobilized on avidin-coated sensor surface. In turn, an order of magnitude lower binding constant was observed in the reversed setup, when C-terminally biotinylated hIFNγ was immobilized in an oriented manner on the avidin-coated sensor and the ABD35-TolA and ABD275-TolA proteins bound from solution. It is plausible to assume that for these two particular ABD variants their binding modes may allow pairs of avidin-immobilized ABD-TolA molecules to bind a single hIFNγ homodimer, thus exhibiting an increased avidity for the target. In turn, no "avidity effect" would be observed with free ABD-TolA molecules binding from a solution to immobilizied hIFNγ homodimers independently of each other. Furthermore, all described ABD variants competed with each other for hIFNγ binding. It appears, therefore, unlikely that only the ABD35 and ABD275 scaffolds are selectively binding to site(s) on hIFNγ that would become less accessible upon oriented immobilization on the avidin-coated chip.

Computational comparison of the surfaces predicted to interact with hIFNγ in various ABDs (Fig. 11) indicated that the core area of their binding surface would be formed by hydrophobic residues and the surrounding area would contain polar and charged residues. The distribution of the latter would, however, vary significantly and a common feature underlying hIFNγ binding could not be clearly identified. This would suggest that the

high affinity of the best binders for hIFNγ may result from a combinatorial interaction of more types of residues, rather than from a major binding motif formed by a structurally predefined consensus. This interpretation would also be supported by the different calculated sizes of the predicted interacting surfaces of ABD variants (Fig. 11), obtained upon structure relaxation of the ABD scaffolds in MD simulations of ABD-hIFNγ complexes. The observed average RMSD values of ABD backbone atoms with respect to the ABD-WT crystal structure reference are 1.61, 1.52, 1.34, and 1.29 Å for ABD35, ABD29, ABD20, and ABD 275, respectively. These values represent the extent of induced geometry change of the ABD structure upon binding to the hIFNγ.

In the case of the ABD29 construct, the binding surface would be enlarged due to increased distance between helices 2 and 3, which may result in location of the helix 1 in closer proximity to the hIFNγ surface (a "flattened" binding mode). Contrary to that, the ABD275 variant is predicted to interact with hIFNγ preferentially through the randomized residues of helix 2, with a minimum interacting contribution of helix 3 (an "oblique" binding mode). This would mean that randomization-mediated sequence changes may control also the orientation of the ligand relative to its target, as suggested in Figure 11. These predictions, however, await experimental testing by determination of the structures of above discussed selected ligands that is currently attempted.

Collectively, the presented results demonstrate the potential of the ABD scaffold to be used for design and selection of novel recombinant ligands of diagnostic or therapeutic targets.

ACKNOWLEDGMENTS

We thank Alena Lehovcová and Petra Kadlčáková for excellent technical assistance.

REFERENCES

1. Muller U, Steinhoff U, Reis LFL, Hemmi S, Pavlovic J, Zinkernagel RM, Aguet M. Functional-role of type-I and type-II interferons in antiviral defense. Science 1994;264:1918–1921.
2. Goodbourn S, Didcock L, Randall RE. Interferons: cell signalling, immune modulation, antiviral response and virus countermeasures. J Gen Virol 2000;81 (Part 10):2341–2364.
3. Randall RE, Goodbourn S. Interferons and viruses: an interplay between induction, signalling, antiviral responses and virus countermeasures. J Gen Virol 2008;89 (Part 1):1–47.
4. Ealick SE, Cook WJ, Vijaykumar S, Carson M, Nagabhushan TL, Trotta PP, Bugg CE. 3-Dimensional structure of recombinant human interferon-gamma. Science 1991;252:698–702.
5. Lunn CA, Davies L, Dalgarno D, Narula SK, Zavodny PJ, Lundell D. An active covalently linked dimer of human interferon-gamma—subunit orientation in the native protein. J Biol Chem 1992;267:17920–17924.
6. Thiel DJ, le Du MH, Walter RL, D'Arcy A, Chene C, Fountoulakis M, Garotta G, Winkler FK, Ealick SE. Observation of an unexpected third receptor molecule in the crystal structure of human interferon-gamma receptor complex. Structure 2000;8:927–936.
7. Binz HK, Pluckthun A. Engineered proteins as specific binding reagents. Curr Opin Biotechnol 2005;16:459–469.
8. Nygren PA, Skerra A. Binding proteins from alternative scaffolds. J Immunol Methods 2004;290:3–28.
9. Skerra A. Alternative non-antibody scaffolds for molecular recognition. Curr Opin Biotechnol 2007;18:295–304.
10. Dennis MS, Lazarus RA. Kunitz domain inhibitors of tissue factor-factor Viia. 1. Potent inhibitors selected from libraries by phage display. J Biol Chem 1994;269:22129–22136.
11. Koide A, Bailey CW, Huang XL, Koide S. The fibronectin type III domain as a scaffold for novel binding proteins. J Mol Biol 1998;284:1141–1151.
12. Nord K, Gunneriusson E, Ringdahl J, Stahl S, Uhlen M, Nygren PA. Binding proteins selected from combinatorial libraries of an alpha-helical bacterial receptor domain. Nat Biotechnol 1997;15:772–777.
13. Nygren PA, Uhlen M. Scaffolds for engineering novel binding sites in proteins. Curr Opin Struct Biol 1997;7:463–469.
14. Hey T, Fiedler E, Rudolph R, Fiedler M. Artificial, non-antibody binding proteins for pharmaceutical and industrial applications. Trends Biotechnol 2005;23:514–522.
15. Hosse RJ, Rothe A, Power BE. A new generation of protein display scaffolds for molecular recognition. Protein Sci 2006;15:14–27.
16. Smith GP. Filamentous fusion phage—novel expression vectors that display cloned antigens on the virion surface. Science 1985;228:1315–1317.
17. Mattheakis LC, Bhatt RR, Dower WJ. An in-vitro polysome display system for identifying ligands from very large peptide libraries. Proc Natl Acad Sci USA 1994;91:9022–9026.
18. Leung DW, Chen E, Goeddel DV. A method for random mutagenesis of a defined DNA segment using a modified polymerase chain reaction. Technique 1989;1:11–15.
19. Forrer P, Binz HK, Stumpp MT, Pluckthun A. Consensus design of repeat proteins. Chembiochem 2004;5:183–189.
20. Binz HK, Stumpp MT, Forrer P, Amstutz P, Pluckthun A. Designing repeat proteins: well-expressed, soluble and stable proteins from combinatorial libraries of consensus ankyrin repeat proteins. J Mol Biol 2003;332:489–503.
21. Stumpp MT, Forrer P, Binz HK, Pluckthun A. Designing repeat proteins: modular leucine-rich repeat protein libraries based on the mammalian ribonuclease inhibitor family. J Mol Biol 2003;332:471–487.
22. Wiederstein M, Sippl MJ. Protein sequence randomization: efficient estimation of protein stability using knowledge-based potentials. J Mol Biol 2005;345:1199–1212.
23. Johansson MU, Frick IM, Nilsson H, Kraulis PJ, Hober S, Jonasson P, Linhult M, Nygren PA, Uhlen M, Bjorck L, Drakenberg T, Forsen S, Wikstrom M. Structure, specificity, and mode of interaction for bacterial albumin-binding modules. J Biol Chem 2002;277:8114–8120.
24. Kraulis PJ, Jonasson P, Nygren PA, Uhlen M, Jendeberg L, Nilsson B, Kordel J. The serum albumin-binding domain of streptococcal protein G is a three-helical bundle: a heteronuclear NMR study. FEBS Lett 1996;378:190–194.
25. Nygren PA, Ljungquist C, Tromborg H, Nustad K, Uhlen M. Species-dependent binding of serum albumins to the streptococcal receptor protein-G. Eur J Biochem 1990;193:143–148.
26. Linhult M, Binz HK, Uhlen M, Hober S. Mutational analysis of the interaction between albumin-binding domain from streptococcal protein G and human serum albumin. Protein Sci 2002;11:206–213.
27. Lejon S, Frick IM, Bjorck L, Wikstrom M, Svensson S. Crystal structure and biological implications of a bacterial albumin binding module in complex with human serum albumin. J Biol Chem 2004;279:42924–42928.
28. Jonsson A, Dogan J, Herne N, Abrahmsen L, Nygren PA. Engineering of a femtomolar affinity binding protein to human serum albumin. Protein Eng Des Sel 2008;21:515–527.

29. Alm T, Yderland L, Nilvebrant J, Halldin A, Hober S. A small bispecific protein selected for orthogonal affinity purification. Biotechnol J 2010;5:605–617.
30. Bendova-Biedermannova L, Hobza P, Vondrasek J. Identifying stabilizing key residues in proteins using interresidue interaction energy matrix. Proteins: Struct Funct Bioinform 2008;72:402–413.
31. Cornell WD, Cieplak P, Bayly CI, Gould IR, Merz KM, Ferguson DM, Spellmeyer DC, Fox T, Caldwell JW, Kollman PA. A second generation force field for the simulation of proteins, nucleic acids, and organic molecules. J Am Chem Soc 1995;117:5179–5197.
32. Case DA, Darden TA, Cheatham TEI, Simmerling CL, Wang J, Duke RE, Luo R, Merz KM, Wang B, Pearlman DA, Crowley M, Brozell S, Tsui V, Gohlke H, Mongan J, Hornak V, Cui G, Beroza P, Schafmeister C, Caldwell JW, Ross WS, Kollman PA. AMBER 8. San Francisco: University of California; 2004.
33. Tsui V, Case DA. Theory and applications of the generalized Born solvation model in macromolecular simulations. Biopolymers 2000;56:275–291.
34. Cavallo L, Kleinjung J, Fraternali F. POPS: a fast algorithm for solvent accessible surface areas at atomic and residue level. Nucleic Acids Res 2003;31:3364–3366.
35. Fraternali F. POPS server, Vol. 2008. Available at: http://mathbio.nimr.mrc.ac.uk/wiki/POPS. Accessed on November 2, 2011.
36. Yin SY, Ding F, Dokholyan NV. Eris: an automated estimator of protein stability. Nat Methods 2007;4:466–467.
37. Yin S, Ding F, Dokholyan NV. Eris protein stability. 2007; Available at: http://eris.dokhlab.org. Accessed on November 2, 2011.
38. Zahnd C, Amstutz P, Pluckthun A. Ribosome display: selecting and evolving proteins in vitro that specifically bind to a target. Nat Methods 2007;4:269–279.
39. Larkin MA, Blackshields G, Brown NP, Chenna R, McGettigan PA, McWilliam H, Valentin F, Wallace IM, Wilm A, Lopez R, Thompson JD, Gibson TJ, Higgins DG. Clustal W and clustal X version 2.0. Bioinformatics 2007;23:2947–2948.
40. Eswar N, John B, Mirkovic N, Fiser A, Ilyin VA, Pieper U, Stuart AC, Marti-Renom MA, Madhusudhan MS, Yerkovich B, Sali A. Tools for comparative protein structure modeling and analysis. Nucleic Acids Res 2003;31:3375–3380.
41. Schymkowitz J, Borg J, Stricher F, Nys R, Rousseau F, Serrano L. The FoldX web server: an online force field. Nucleic Acids Res 2005;33:W382–W388.
42. Comeau SR, Kozakov D, Brenke R, Shen Y, Beglov D, Vajda S. ClusPro: performance in CAPRI rounds 6-11 and the new server. Proteins: Struct Funct Bioinform 2007;69:781–785.
43. Hess B, Kutzner C, van der Spoel D, Lindahl E. GROMACS 4: algorithms for highly efficient, load-balanced, and scalable molecular simulation. J Chem Theory Comput 2008;4:435–447.
44. Duan Y, Wu C, Chowdhury S, Lee MC, Xiong GM, Zhang W, Yang R, Cieplak P, Luo R, Lee T, Caldwell J, Wang JM, Kollman P. A point-charge force field for molecular mechanics simulations of proteins based on condensed-phase quantum mechanical calculations. J Comput Chem 2003;24:1999–2012.
45. Vaisocherová H, Zítová A, Lachmanová M, Štěpánek J, Králíková S, Liboska R, Rejman D, Rosenberg I, Homola J. Investigating oligonucleotide hybridization at subnanomolar level by surface plasmon resonance biosensor method. Biopolymers 2006;82:394–398.
46. Vaisocherová H, Snášel J, Špringer T, Šípová H, Rosenberg I, Štěpánek J, Homola J. Surface plasmon resonance study on HIV-1 integrase strand transfer activity. Anal Bioanal Chem 2009;393:1165–1172.
47. Ansari S, Helms V. Statistical analysis of predominantly transient protein-protein interfaces. Proteins: Struct Funct Bioinform 2005;61:344–355.
48. Glaser F, Steinberg DM, Vakser IA, Ben-Tal N. Residue frequencies and pairing preferences at protein-protein interfaces. Proteins: Struct Funct Genet 2001;43:89–102.
49. Yin S, Ding F, Dokholyan NV. Modeling backbone flexibility improves protein stability estimation. Structure 2007;15:1567–1576.
50. Fountoulakis M, Juranville JF, Stuber D, Weibel EK, Garotta G. Purification and biochemical-characterization of a soluble human interferon-gamma receptor expressed in *Escherichia coli*. J Biol Chem 1990;265:13268–13275.
51. Nord K, Nilsson J, Nilsson B, Uhlen M, Nygren PA. A combinatorial library of an alpha-helical bacterial receptor domain. Protein Eng 1995;8:601–608.
52. Nord K, Nord O, Uhlen M, Kelley B, Ljungqvist C, Nygren PA. Recombinant human factor VIII-specific affinity ligands selected from phage-displayed combinatorial libraries of protein A. Eur J Biochem 2001;268:4269–4277.
53. Kronqvist N, Malm M, Gostring L, Gunneriusson E, Nilsson M, Guthenberg IH, Gedda L, Frejd FY, Stahl S, Lofblom J. Combining phage and staphylococcal surface display for generation of ErbB3-specific affibody molecules. Protein Eng Des Sel 2011;24:385–396.